Philosophical Magazine A, 2002, Vol. 82, No. 4, 685–698

Taylor & Francis
Taylor & Francis Group

Stacking faults and twins in gallium phosphide layers grown on silicon

V. Narayanan†, S. Mahajan‡

Department of Chemical and Materials Engineering and Center for Solid State Electronics Research, Arizona State University, Tempe, Arizona 85287-6006, USA

K. J. Bachmann

Department of Materials Science and Engineering, North Carolina State University, Raleigh, North Carolina 27695-7919, USA

V. Woods and N. Dietz

Department of Physics, North Carolina State University, Raleigh, North Carolina 27695-7919, USA

[*Received 23 February 2001 and accepted in revised form 25 June 2001*]

Abstract

The coalescence of GaP islands, grown on Si(001), Si(111), Si(110) and Si(113) surfaces by chemical beam epitaxy, has been investigated by high-resolution transmission electron microscopy. Stacking faults and first-order twins are observed within islands before coalescence and result from stacking errors during growth on the smaller P-terminated {111} facets of GaP islands. Upon island coalescence, complex moiré fringes are observed contiguous to highly faulted {111} planes within epitaxial layers grown on all four Si substrate orientations and are attributed to multiple twinning. Second- and third-order twins are also observed within (111) and (110) layers and their formation is attributed to successive twinning on differently inclined {111} facets. Amongst the four orientations, coalesced growths on the Si(111) surface are the most defective and this may be caused by a higher density of P-terminated {111} facets on islands grown on the Si(111) surface.

§ 1. Introduction

GaP epitaxial layers (epilayers) grown on Si are nearly ideal to study the effects of substrate orientation on the growth morphology and defect microstructure during polar on non-polar heteroepitaxy because of the low lattice mismatch (0.37%). In a recent study we showed that GaP nucleated as facetted three-dimensional (3D) islands on the Si(001) and Si(111) surfaces, while a nearly two-dimensional (2D) growth mode was seen on the Si(110) and Si(113) surfaces (Narayanan *et al.* 2000). The change in growth mode was attributed to the absence of charge build-

† Present address: IBM T. J Watson Research Center, Yorktown Heights, New York 10598, USA. Email: vijayna@us.ibm.com
‡ Email: smahajan@asu.edu

Philosophical Magazine A ISSN 0141–8610 print/ISSN 1460-6992 online © 2002 Taylor & Francis Ltd
http://www.tandf.co.uk/journals
DOI: 10.1080/01418610110082034

up at the GaP–Si heterointerface for the (110) and (113) orientations, thereby reducing the interface energy. Furthermore, stacking errors on {111} facets of epitaxial islands led to a high density of stacking faults (SFs) and first-order twins (Ernst and Pirouz 1988, 1989, Narayanan *et al.* 1999, 2000) with propensity of faulting more pronounced on the smaller P-terminated {111} facet (Narayanan *et al.* 1999, 2000). The observation of a more uniform 2D growth mode for the (110) and (113) surfaces suggested that growth on these two Si surfaces may provide a plausible way of reducing the planar defect density in the coalesced GaP epitaxial films grown on Si. However, the question of what happens to the defect density after island coalescence is still unresolved.

In this paper, we have investigated defects within GaP epilayers after island coalescence on all four aforementioned Si substrate orientations using cross-sectional high-resolution transmission electron microscopy (HRTEM). The emphasis is on the evolution of defects within epilayers by comparing the microstructures of growths on Si(001) and Si(111) with Si(110) and Si(113) surfaces.

§ 2. Experimental procedure

The Si(001), Si(111), Si(110) and Si(113) wafers were cleaned using a standard RCA clean (Narayanan *et al.* 2000). GaP was deposited on Si substrates using pulsed chemical beam epitaxy (Kelliher *et al.* 1993), wherein the heated Si substrate was exposed to pulses of *tert*-butylphosphine (TBP) and triethylgallium (TEG) under a steady activated H_2 background pressure (Bachmann *et al.* 1995, Narayanan *et al.* 2000). The overall pressure during deposition was between 10^{-4} and 10^{-5} Torr and the layers were grown within a temperature range 350–560°C. Using a cycle time of 5 s, TEG flow of 0.05 sccm was pulsed into the reactor for 300 ms per cycle under continuous TBP and H_2 flows of 0.6 and 5.0 sccm respectively.

Samples for transmission electron microscopy (TEM) were prepared using the standard 'sandwich' techniques followed by dimpling and ion milling until electron transparency. Structural analysis of the epitaxial layers was performed in cross-section on a JEM-4000EX microscope operating at 400 kV that has an interpretable resolution of 0.16 nm. Localized spatial information from high-resolution transmission electron micrographs was obtained by digital diffractograms (DDFs). The method is based on measurements of interplanar spacings in reciprocal space and can be used to determine the frequency and amplitude of lattice images. Since each fringe in a high-resolution lattice image corresponds to a characteristic spot in the amplitude of the Fourier transform (diffractogram) of a selected image region, lattice-fringe spacings and angles can be measured from spot positions with respect to the centre of the diffractogram. Calculation of diffractograms has been discussed in detail by De Rujiter *et al.* (1995) and the reader is referred to that article for additional information.

§ 3. General observations

Figures 1 (*a*) and (*b*) show HRTEM images of GaP(001) epilayers grown for 500 s at 420 and 560°C respectively. SFs and twins on {111} planes are the dominant features of these epilayers. SFs are observed to terminate within the epilayer (S_1), to intersect with other SFs (S_3 and S_4; S_5 and S_6) and to intersect with microtwins (S_2 and T_1). In addition to these SFs, a defect A1 is observed in figure 1 (*a*). This defect is identified as an antiphase boundary and has been discussed elsewhere (Narayanan

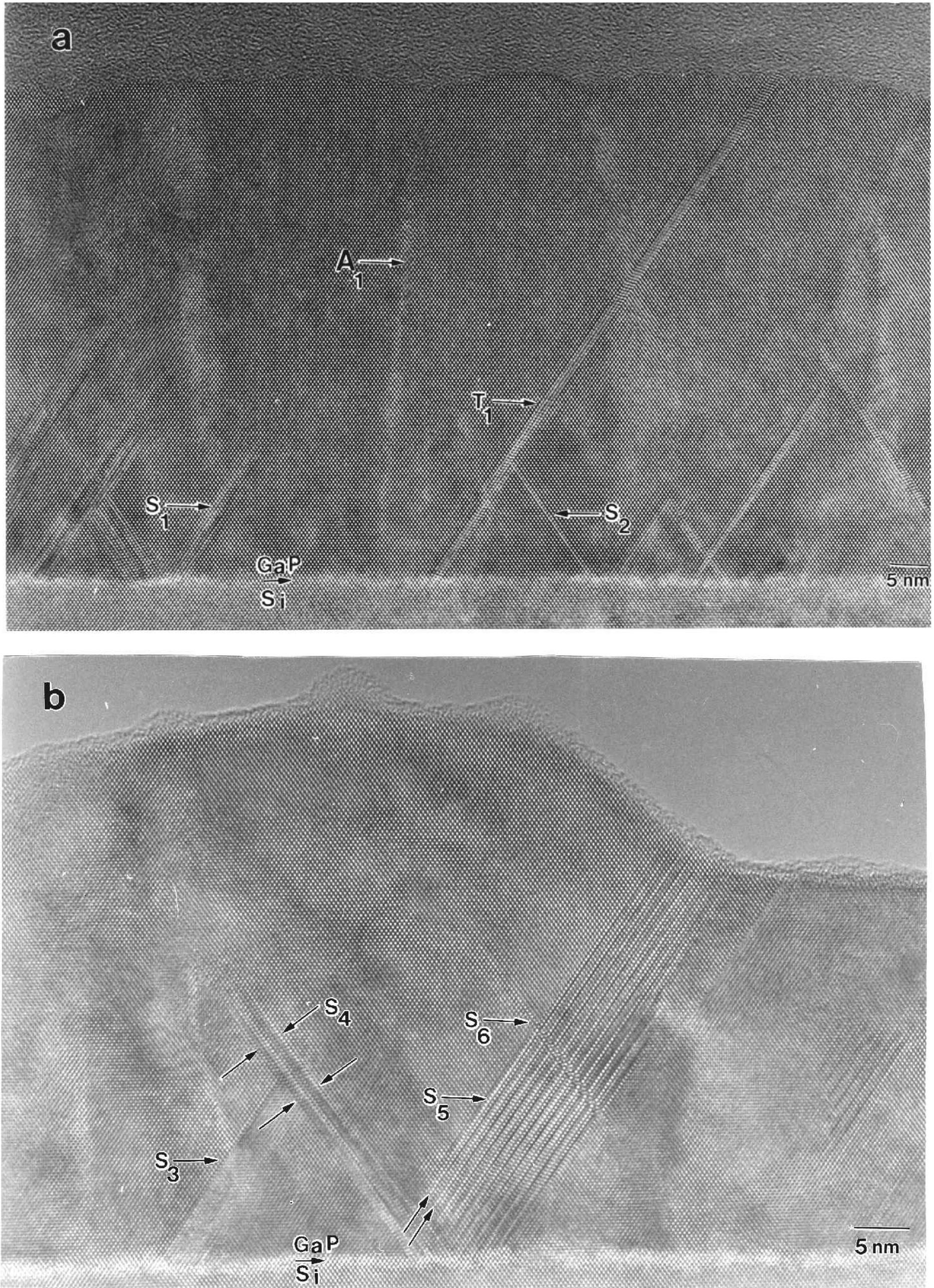

Figure 1. (*a*) HRTEM image of a GaP epilayer grown on Si(001) after growth for 500 s at 420°C. (*b*) HRTEM image of a GaP epilayer grown on Si(001) after growth for 500 s at 560°C.

1999). Comparing the morphology of the two layers, the epilayer surface is rougher at 560°C.

Figure 2 shows HRTEM images of GaP{111} epilayers grown for 300 s at 420°C. In figure 2(*a*), the matrix M twins on a {111} facet parallel to the interface to

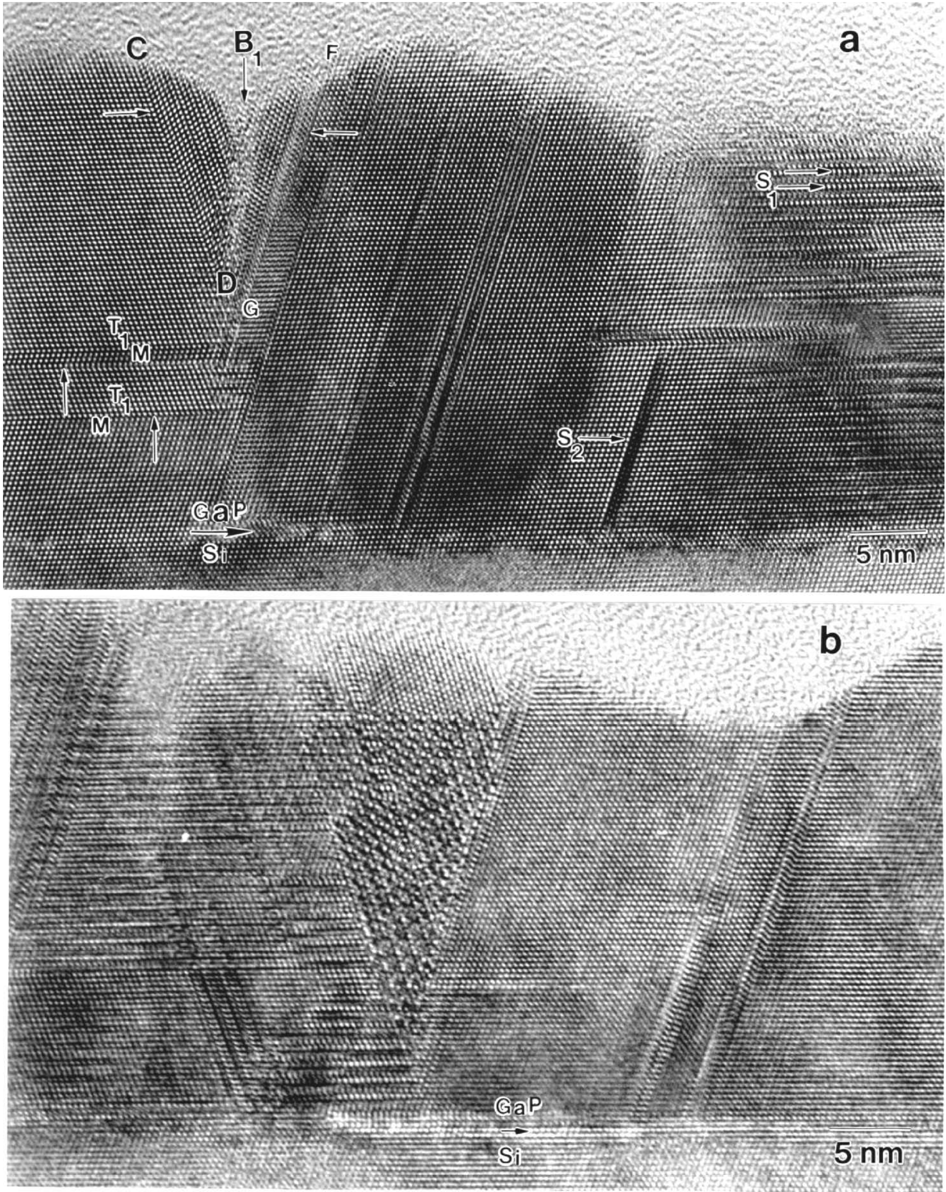

Figure 2. (*a*), (*b*) HRTEM images of GaP epilayers grown on Si(111) after growth for 300 s at 420°C.

produce T_1, which again twins on the same facet back to the M orientation. This operation is repeated again as indicated in the figure. Figure 2 (*a*) also indicates that continuous twinning on island facets CD and FG can produce a subgrain boundary B_1 after island coalescence. Towards the right of this figure, highly faulted {111} regions denoted by S_1 are also observed. Figure 2 (*b*) shows regions of complex contrast (in the shape of a V) contiguous to the highly faulted {111} planes that are parallel to the interface. Both figure 2 (*a*) and figure 2 (*b*) show a rough surface morphology. The highly faulted areas are also observed in a thick (110) epilayer

grown for 2200 s at 420°C (figure 3). The inset in figure 3 is the associated selected-area diffraction pattern (SADP) that clearly show twin spots arranged in a regular manner at one third and two thirds of the distance from the transmitted spot to each of the fundamental reflections of GaP. The HRTEM image also shows regions of complex contrast at the intersection of highly faulted regions that lie on inclined planes.

Figures 4 (*a*) and (*b*) are HRTEM images of GaP(001) and GaP(111) epilayers grown at 350 and 420°C for 500 and 300 s respectively, with corresponding DDFs

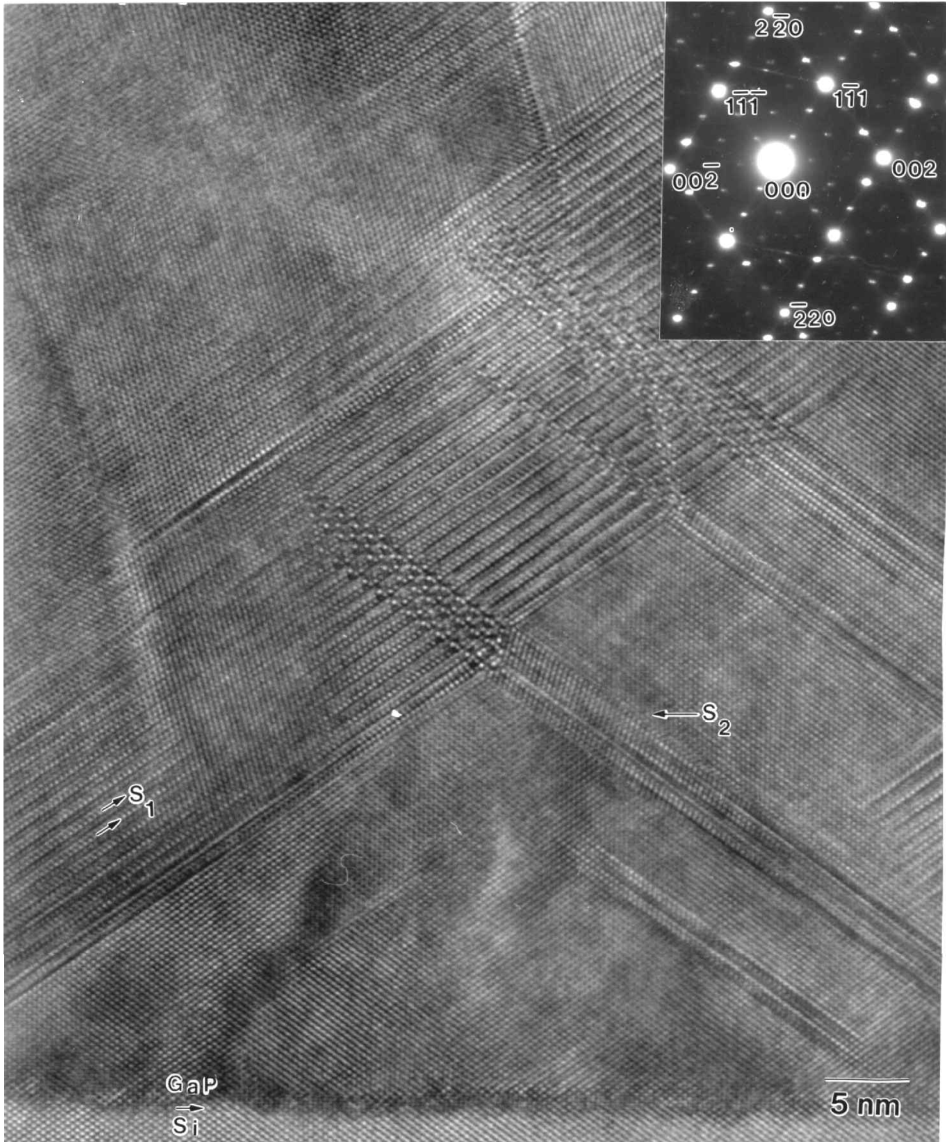

Figure 3. HRTEM image of a GaP epilayer on Si(110) after growth for 2200 s at 420°C. The inset is the SADP of the GaP(110) epilayer that shows both twin and doubly diffracted spots.

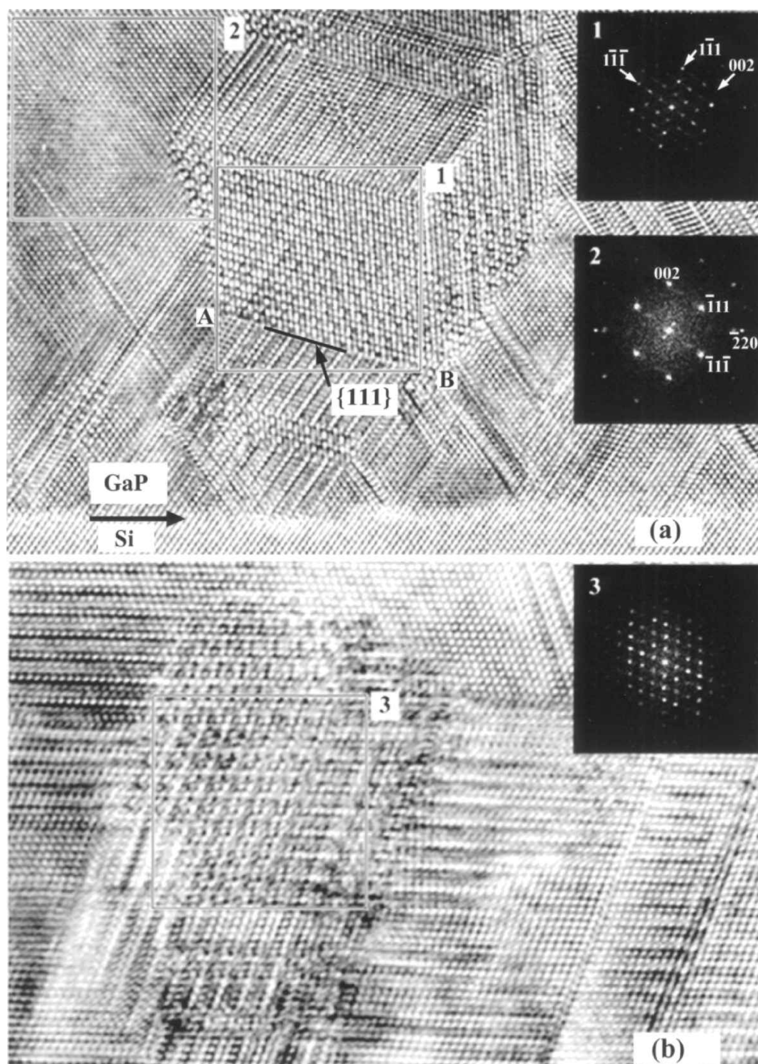

Figure 4. (*a*) and (*b*) show areas of complex contrast on (001) (350°C and 500 s of growth) and Si(111) (420°C and 300 s of growth), respectively. The insets are DDFs obtained from the selected areas.

shown as insets in the figure. DDFs 1 and 3 are taken from regions that exhibit complex contrast. DDF 2 gives reciprocal-space information from areas that exhibit no defects. Upon comparing DDFs 1 and 2 in figure 4 (*a*), it is observed that the former is rotated by 70.5° from the latter. In addition, the DDFs 1 and 3 show the presence of twin spots at positions nearly identical with those seen in the SADP of figure 3. Further examination of figure 4 (*a*) shows that AB is the trace of {111} planes from the regions of complex contrast above AB and {111} planes in the faulted regions below AB. Similarly oriented traces are observed in different locations within the image.

Figures 5 (*a*) and (*b*) are HRTEM images of GaP(110) and GaP(113) epilayers grown at 420°C for 2200 and 2300 s respectively. All the DDFs obtained from the

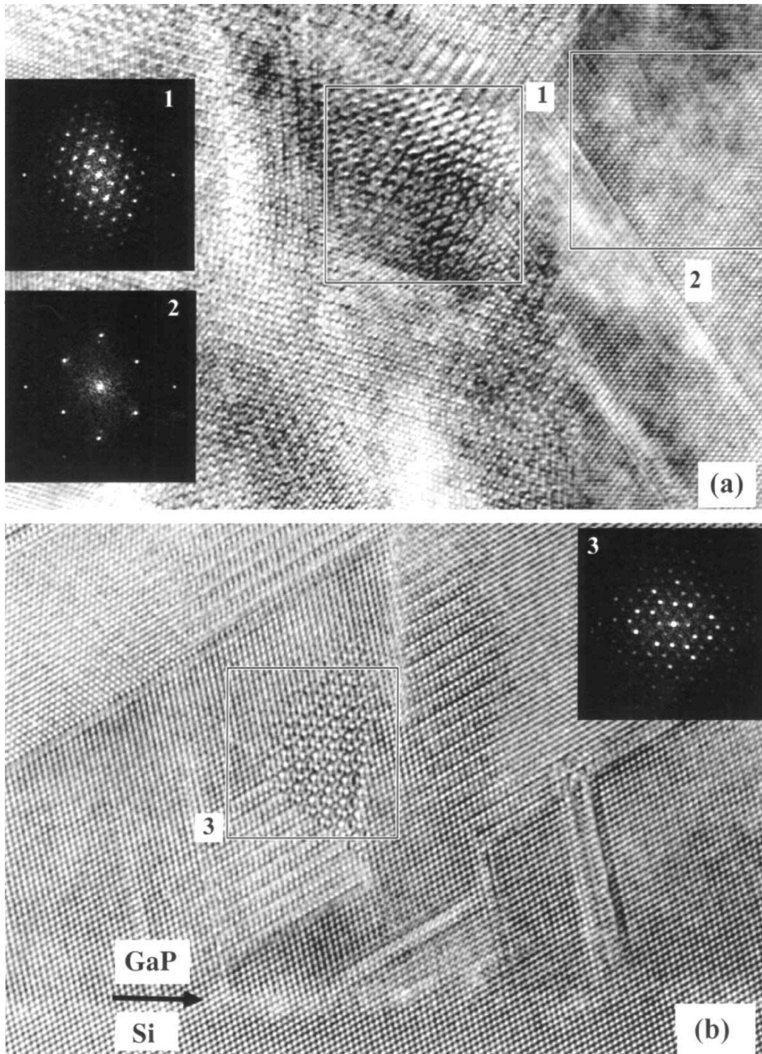

Figure 5. Areas of complex contrast on (*a*) Si(110) (growth for 2200 s at 420°C) and (*b*) Si(113) (growth for 2300 s at 420°C). The insets are DDFs obtained from selected areas.

regions of complex contrast in these images show satellite spots similar to those seen in figures 3 and 4. Comparing the faulted microstructures of the {113} and {111} epilayers, it is inferred that faulting is more prevalent on the shallowly inclined {111} planes. In addition, the regions of complex contrast are mostly observed either contiguous to the highly faulted segments (figures 2 (*b*), 4 (*a*) and 5 (*b*)) or at the intersection of highly faulted segments (figure 3).

Figure 6 is a HRTEM image of a GaP epilayer grown on Si(110) at 420°C. The micrograph indicates two large-angle tilt boundaries labelled 1A and 1B. The boundary 1A is identified in the coincident-site lattice terminology as a $\Sigma = 9$, $(221)[1\bar{1}0]$, $\theta = 38.96°$ symmetric tilt boundary, otherwise known as a second-order twin (Holt 1984). This was ascertained by calculating the rotation across the boundary and mapping out the trace of the boundary plane on either side. The boundary 1B is

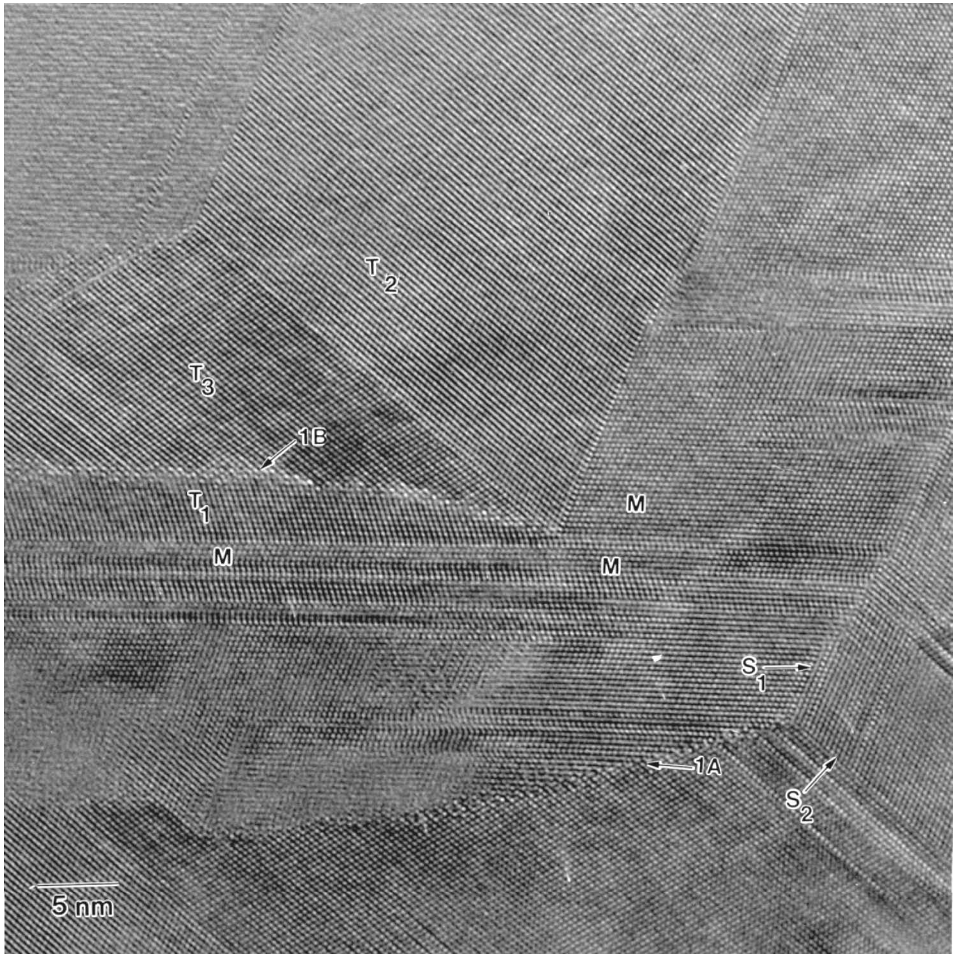

Figure 6. HRTEM image of large-angle tilt boundaries within a GaP epilayer grown on Si(110) after growth for 2200 s at 420°C.

identified as $\Sigma = 27$ with a tilt of 31.58° about [1$\bar{1}$0] (the tilt is measured across the boundary). This boundary in the symmetrical form is called a third-order twin. SFs S_1 and S_2 and twins T_1, T_2 and T_3 are also observed. Figures 7 (*a*) and (*b*) show HRTEM images of GaP epilayers grown on Si(111) at 420°C for 600 s. It was concluded that features 1A and 1B are large-angle tilt boundaries that were also seen within GaP growths on Si(110).

§ 4. Discussion

Several significant observations emerge from the present study. Firstly, epitaxial films develop a rougher morphology and have larger thicknesses with increasing temperature. Secondly, large volumes of highly faulted areas and regions of complex contrast contiguous to these faulted areas are observed for all four GaP orientations. Thirdly, large-angle tilt boundaries form within GaP epilayers grown on Si(110) and Si(111).

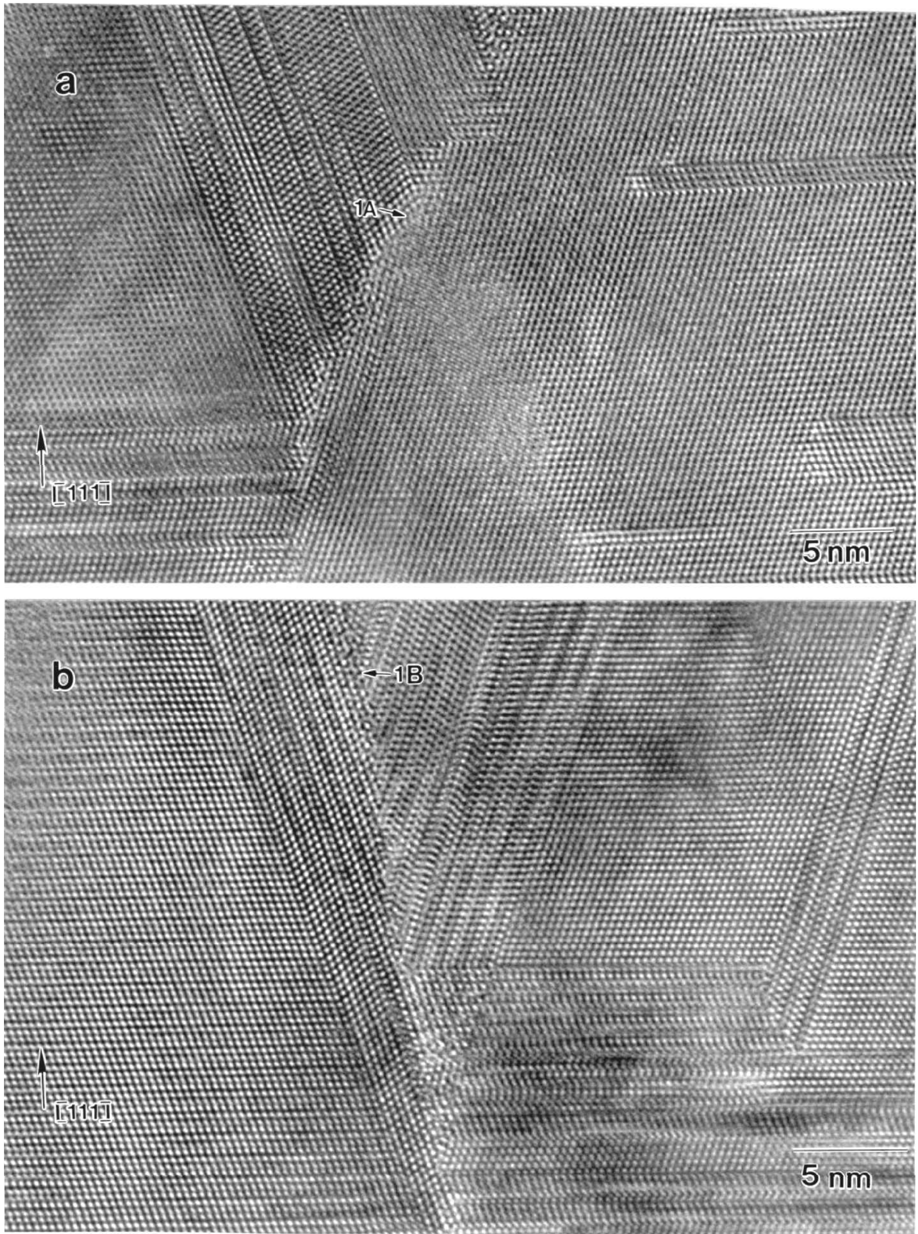

Figure 7. (*a*), (*b*) HRTEM images of large-angle tilt boundaries within a GaP epilayer grown on Si(111) after growth for 600 s at 420°C.

Figures 1 (*a*) and (*b*) show that films grown at higher temperatures are rougher. This observation agrees with our earlier results (Narayanan *et al*. 2000) that the layers nucleate as facetted 3D islands which are larger, have different heights, are more facetted and fewer in number at higher growth temperatures. The coalescence of such islands would lead to rougher epilayers.

In figure 1 (*a*) some of the SFs (e.g. S_1) do not propagate through the film. This may be because, as we move away from the interface, the misfit-induced shear stress on the fault plane may fall below the critical resolved shear stress required for glide. Thus it is expected in a low-lattice-mismatch system, such as GaP–Si, that the glide of Shockley partials is limited and the faults may terminate within the film. Figures 1 (*a*) and (*b*) show a SF S_2 that intersects with T_1, and a SF S_3 that intersects with S_4, resulting in either the thickening or the unfaulting of T_1 and S_4. This is attributed to the glide of Shockley partials that form as a result of stair-rod cross-slip at the intersection of crossing and crossed faults (Mahajan and Chin 1973). Highly faulted regions are also observed within all four epilayers and are observed mostly on {111} planes which are *shallowly inclined* to the growth interface, suggesting that shallow {111} facets provide a better template for faulting than steep facets do. This can be rationalized in terms of the larger projected areas of shallow {111} facets exposed to incoming adatoms, facilitating the formation of a high density of continuous faults.

A common feature in GaP epilayers is the observation of regions of complex contrast for all four substrate orientations. Among the four orientations, GaP(110) epilayers show the highest density of these features. A SADP of this film is shown in the inset of figure 3. Besides the main spots characteristic of the zincblende [110] diffraction pattern (some of which are indexed), additional twin spots are present. DDFs from regions of complex contrast in GaP(001), GaP(111), GaP(110) and GaP(113) layers in figure 4 and figure 5 also show twin spots nearly identical with the SADP of figure 3. The DDFs have also revealed a twin relationship between the regions of complex contrast and the matrix as discussed earlier. The presence of twins in these layers results in additional spots in the diffraction pattern (observed as bright spots besides fundamental reflections in the SADP in figure 3). The diffracted beams due to the inclined twins may then act as incident beams for the GaP matrix, resulting in the doubly diffracted spots in the SADP in figure 3 (they are observed as spots that are weaker in intensity). Thus, we believe that the spots in the DDFs and the regions of complex contrast in the HRTEM images are due to the presence of localized twins or faults that do not propagate through the thickness of the TEM foil such that the observed features are complex moiré fringes that form owing to the superposition of doubly diffracted beams from both the matrix and the faulted regions. These localized multiply twinned regions are facilitated at the intersection of highly faulted {111} segments (figure 3) because of possible stress concentration, a result consistent with the work of Dahmen *et al.* (1990) and Pirouz *et al.* (1990) on twin–twin intersections in hot indented Si which resulted in the formation of a hexagonal Si phase.

Another interesting observation is the formation of large-angle tilt boundaries identified as second- and third-order twins within GaP(110) (figure 6) and GaP(111) (figure 7) films. We believe that second- and third-order twins within our GaP epilayers are formed because of successive twinning on different {111} planes. Twinning in the zincblende structure can be produced by twofold (180°) rotations about the $\langle 111 \rangle$ axes. One such rotation produces a first-order twin orientation. Two successive rotations about two different $\langle 111 \rangle$ axes produce a second-order twin when the two growths coalesce. Such a twinning operation occurs at the boundary 1A in figure 6 and is also observed in GaP(111) layers in figure 7 (*a*).

Third-order twins are also observed in figure 6 and are labelled 1B. A twinning operation on a {111} facet of the matrix M produces the twin T_1. This twin on the

right-hand side of the image undergoes a twinning operation on the same {111} plane again to reach the matrix orientation. Twinning on the other {111} facet within M produces the twin T_2. A similar twin operation on the other {111} plane of T_2 produces T_3. The boundary between T_1 and T_3 is then a $\Sigma = 27$ boundary. The curved and stepped regions make it difficult to determine the boundary plane, although we do expect symmetric and asymmetric components which could further dissociate into other low-energy configurations (Merkle and Wolf 1992). Third-order twins are also observed in GaP(111) layers in figure 7 (*b*). Figure 2 (*a*) (left-hand, B_1) also clearly indicates that the coalescence of epitaxial islands facetted on different twinned {111} planes can lead to the formation of subgrain boundaries. Within the areas sampled by TEM, both the (001) and the (113) surfaces do not exhibit such large-angle boundaries in layers grown at 420°C.

Second-order twins have been observed previously in semiconductor structures such as Si ribbons deposited on Mo substrates (Cunningham and Ast 1982), Czochralski grown Ge crystals tilted so as to produce such twins (Papon *et al.* 1982), and GaAs layers grown on Ge bicrystals to create particular grain boundaries artificially (Carter *et al.* 1985, De Cooman *et al.* 1985). In epitaxial films, similar tilt boundary structures are observed much less frequently. They have been shown to occur in GaAs/Si(001) grown by low-pressure metal-organic vapour-phase deposition (Meddeb *et al.* 1993). These workers also attributed the formation of these grain boundaries to successive twinning. {221} V-shaped defects have been observed at the surface of Ge epitaxial films grown on Si(001) (Legoues *et al.* 1989). These Ge layers were forced to grow in the layer-by-layer growth mode and islanding was prevented even after 14–16 monolayers of growth. With increasing layer thickness, there is a very large driving force to relieve the lattice misfit strain and the observed defects are created catastrophically throughout the film. Legoues *et al.* have attributed the formation of second order twins to a strain relief mechanism. Similar V-shaped {221}-type wedge defects have also recently been observed in $Si_{1-x}Ge_x$ grown on Si(001) (Mullner *et al.* 1997, Ozkan *et al.* 1997, Gao *et al.* 1999), where the formation of the wedge is attributed to local stress concentration during growth. Thus, although higher-order twins are rarely observed in semiconductor epitaxy, they can occur under some extraneous circumstances.

Results show that planar defect density including SFs, twins and tilt boundaries is lower in GaP layers grown on (001) compared with (111) for the same growth temperature. Since P forms stronger bonds to Si (Uhrberg *et al.* 1986, Kaxiras 1995) the Si surface will mostly be P terminated. The lower surface mobility for incoming adatoms due to the higher dangling bond density of a P-terminated Si(111) surface compared with a Ga-terminated Si(111) surface causes the incoming adatoms to be immobilized as they land and not to reach their equilibrium positions. Thus, on the (111) surface, the substrate orientation acts as a template for the formation of growth defects such as microtwins and SFs. This leads to a high defect density at an early stage within epitaxial islands.

GaP growth nucleates on Si(001) as elongated truncated prismatic islands with two P-terminated {111} facets and two Ga-terminated {111} facets (the anisotropy in shape arises from differences in surface energy of P- and Ga-terminated {111} surfaces respectively) and on Si(111) as hexagonal islands with unequal parallel sides that have three P-terminated {111} inclined facets and three Ga-terminated {111} inclined facets (Narayanan *et al.* 2000). Thus, coalescence of islands grown on Si(111) with twinned $\{\bar{1}\bar{1}\bar{1}\}_P$ facets could lead to the evolution of tilt boundaries

during island coalescence. This may explain the observations in figures 2 and 7. Our results have also shown that island coalescence does not produce second- or third-order twins for growth on Si(001) at 350, 420 or 560°C (at least within the areas observed by TEM). This could be attributed to the fewer number of P-terminated {111} facets per island for islands grown on Si(001) compared with islands grown on the Si(111) surface (two versus four). However, it must be stated that these island shapes are idealized situations based on the assumption that the islands are facetted only on {111} planes. Our earlier experimental work (Narayanan *et al.* 2000) had shown that, while the GaP islands on both Si(001) and Si(111) were primarily facetted on {111} planes, a number of islands had higher-index non-polar {112}- and {113}-type facets that were stabilized by charge considerations. Indeed, islands that were facetted on such planes did not show a high incidence of SFs and twins and are thus not expected to result in subboundary formation upon island coalescence.

GaP growths on both Si(110) and Si(113) show a high density of microtwins and SFs. However, within the areas of the films observed by TEM, large-angle tilt boundaries are seen only in epilayers grown on Si(110). For the (110) surface, two of the four {111} planes shallowly inclined to the (110) surface (35.24°) and two of the planes are inclined 90° to the surface. The shallow facets (1$\bar{1}$1) and (1$\bar{1}\bar{1}$) are terminated by P and Ga atoms respectively. Low-magnification images (Narayanan 1999) have revealed a higher propensity for faulting on one of the two shallowly inclined {111} planes, implying that this may be P terminated. In the case of the (113) surface, only one out of the four {111} planes has a shallow inclination. 2D and 3D islands would tend to facet along shallowly inclined {111} facets. In addition, faulting though possible on the steep facet appears to be more localized and less ubiquitous. Since there are a larger number of {111} facets at shallow incidence for faulting in the case of growth on Si(110) compared with Si(113), it is envisaged that these epilayers would exhibit a higher planar defect density.

Microstructurally, the difference between the four orientations can be attributed to the number of P-terminated, shallowly inclined facets. Comparison of the microstructure of epilayers on the four orientations has revealed that epitaxial growth on the Si(001) and Si(113) surfaces produces the least defective epilayer microstructures. Among GaP growths on Si(110) and Si(111), the complex shape of islands on Si(111) could lead to added difficulties during coalescence. Thus growths on the Si(111) surface are expected to be the most defective.

§5. Conclusions

(1) Complex moiré-like features have been observed in GaP films grown on the (001), (111), (110) and (113) surfaces of Si. The moiré fringes are attributed to localized multiple twinning on {111} facets and the superposition of doubly diffracted beams from both the twin and the matrix. In addition, second- and third-order twins have been seen for growths on Si{111} and Si{110}. This is a result of successive twinning on differently inclined {111} facets.

(2) SFs and twins are observed within coalesced GaP growths on Si(001), Si(111), Si(110) and Si(113) substrates. The GaP(001) epilayers show a lower density of SFs than the GaP(111) epilayers do. This is attributed to fewer $\{\bar{1}\bar{1}\bar{1}\}_P$ facets per island for the (001) surface. GaP epilayers grown on Si(110) are more defective than growths on the Si(113) surface. This is a

result of a higher number of shallowly inclined {111} facets for the (110) surface. For growths on the {111} surface, results clearly show that island coalescence increases the planar defect density because of the formation of large-angle tilt boundaries that are attributed to twinning on {111} facets of different islands.

(3) The formation of {111} facets whether on 2D or 3D islands is detrimental to the structural quality of the epitaxial films as it increases the propensity to form SFs and twins. This explains the highly defective morphology within films grown on all four Si orientations independent of interface polarity.

Acknowledgements

V.N. and S.M. would like to acknowledge the Centre for High Resolution Electron Microscopy at Arizona State University for the use of TEM and computing facilities. All the authors would like to acknowledge gratefully the support of this work by US Department of Defense Multidisciplinary University Research Initiative (MURI) grant F49620-95-1-0447.

References

Bachmann, K. J., Rossow, U., and Dietz, N., 1995, *Mater. Sci. Engng.,* **B35**, 472.

Carter, C. B., Cho, N. H., Elgat, Z., Fletcher R., and Wagner D. K., 1985, *Microscopy of Semiconducting Materials 1985,* Institute of Physics Conference Series, Vol. 65, edited by A. G. Cullis and D. B. Holt (Bristol: Institute of Physics), pp. 221–226.

Cunningham, B., and Ast, D., 1982, *Grain Boundaries in Semiconductors,* Materials Research Society Symposium Proceedings, Vol. 5, edited by H. J. Leamy, G. E. Pike and C. H. Seager (Pittsburgh, Pennsylvania: Materials Research Society), pp. 21–26.

Dahmen, U., Westmacott, K. H., Pirouz, P., and Chaim, R., 1990, *Acta metall. mater.,* **38**, 323.

De Cooman, B. C., Cho, N. H., Elgat, Z., and Carter, C. B., 1985, *Ultramicroscopy,* **18**, 305.

De Rujiter, W. J., Sharma, R., McCartney, M. R., and Smith, D. J., 1995, *Ultramicroscopy,* **57**, 409.

Ernst, F., and Pirouz, P., 1988, *J. appl. Phys.,* **64**, 4526; 1989, *J. Mater. Res.,* **4**, 834.

Gao, H., Ozkan, C. S., Nix, W. D., Zimmerman, J. A., and Freund, L. B., 1999, *Phil. Mag.* A, **79**, 349.

Holt, D. B., 1984, *J. Mater. Sci.,* **19**, 439.

Kaxiras, E., 1995, *Mater. Sci. Engng.,* **B30**, 175.

Kelliher, J. T., Thornton, J., Dietz, N., Lucovsky, G., and Bachmann, K. J., 1993, *Mater. Sci. Engng.,* **B22, 97.**

LeGoues, F. K., Copel, M., and Tromp, R., 1989, *Phys. Rev. Lett.,* **63**, 1826.

Mahajan, S., and Chin, G. Y., 1974, *Acta metall.,* **22**, 1113.

Meddeb, J., Ambri, M., Pitaval, M., Draidia, N., Dieter, R. J., and Scholz, F., 1993, *Microscopy of Semiconducting Materials 1993*, Institute of Physics Conference Series, Vol. 134, edited by A. G. Cullis, A. E. Staton-Bevan and J. L. Hutchison (Bristol: Institute of Physics), pp. 361–364.

Merkle, K. L., and Wolf, D., 1992, *Phil. Mag.* A, **65**, 513.

Mullner, P., Gao, H., and Ozkan, C. S., 1997, *Phil. Mag.* A, **75**, 925.

Narayanan, V., 1999, PhD Thesis, Carnegie Mellon University, Pittsburgh, Pennsylvania.

Narayanan, V., Mahajan, S., Sukidi N., Bachmann, K. J., Woods, V., and Dietz, N., 2000, *Phil. Mag.* A, **80**, 555.

Narayanan, V., Sukidi N., Bachmann, K. J., and Mahajan, S., 1999, *Thin Solid Films,* **357**, 53.

Ozkan, C. S., Nix, W.D., and Gao, H., 1997, *Defects in Electronic Materials II,* Materials Research Society Symposium Proceedings, Vol. 442, edited by J. Michel (Pittsburgh, Pennsylvania: Materials Research Society), pp. 373–379.

Papon, A. M., Petit, M, Silvestre, G., and Bacmann, J. J., 1982, *Grain Boundaries in Semiconductors,* Materials Research Society Symposium Proceedings, Vol. 5, edited by H. J. Leamy, G. E. Pike and C. H. Seager (Pittsburgh, Pennsylvania: Materials Research Society), pp. 27–32.

Pirouz, P., Chaim, R., Dahmen, U., and Westmacott, K. H., 1990, *Acta metall. mater.,* **38**, 313.

Uhrberg, R. I. G., Bringans, R. D., Bachrach, R. Z., and Northrup, J. E., 1986, *J. vac. Sci. Technol.* A, **4**, 1259.